La mer 31: 59–78, 1993
Société franco-japonaise d'océanographie, Tokyo

Dispersion of passive tracers in an oceanic mesoscale eddy field*

Keiko YOKOYAMA**, *** and Kenzo TAKANO**

Abstract: Numerical experiments are carried out for estimating the effect of the mesoscale eddies on the dispersion of dynamically passive tracers in a model ocean. Tracers are dispersed by advection and diffusion. The velocity field is supplied as a function of time from a prognostic, four-level, eddy resolving ocean circulation model. The model ocean extending from 25.0°N to 50.5°N in latitude and over 24.8° in longitude may be considered as a portion of the northwestern Pacific Ocean of simplified geometry. Its depth is 4000m except at a ridge 1900m high. The grid size is 0.375° in latitude and 0.43° in longitude. The substance concentration is calculated at depths of 80, 400, 1600 and 2600m by integrating in time a three-dimensional advection-diffusion equation.

The large scale dispersion over the whole ocean basin is shown in two cases; one is the dispersion from an instantaneous plane source distributed over the whole ocean surface, and the other is the dispersion from an instantaneous point source on the bottom. The coefficient of horizontal diffusion is $10^3 m^2/s$. The coefficient of vertical diffusion is $10^{-4} m^2/s$. The complete dispersion defined by the uniform distribution of tracers over the whole ocean basin is achieved in about 30 years in both cases. If the time-average velocity field is used instead of the eddy field, it is achieved in about 50 years. The dispersion is significantly enhanced by mesoscale eddies. Since the time required for the complete dispersion depends on the volume of the ocean basin, and the volume of the model ocean is $1.77 \times 10^7 km^3$ compared with $72.4 \times 10^7 km^3$ of the Pacific Ocean and $137 \times 10^7 km^3$ of the world ocean, a simulated period of 30 years should be equivalent to 1250 years in the Pacific Ocean and 2310 years in the world ocean. Both figures surprisingly agree with the turnover time estimated from ^{14}C and others.

1. Introduction

The ocean interior is filled with velocity fluctuations having horizontal scales of some hundreds of kilometers, vertical scales approximately equal to the water depth and time scales of several weeks, which are commonly referred to as mesoscale eddies. Their typical phase velocity is about 10cm/s. The typical particle velocity is also about 10cm/s. Since the time-average is about 1cm/s or less, the eddy kinetic energy is predominant in the mid-ocean kinetic energy.

The eddy-induced dispersion has important oceanographic consequences in a wide range of fields. It is linked to the general circulation through the transport of momentum, heat and salt and to the ocean-atmosphere system through the transport of heat, water (salt) and carbon dioxide, to biological productivity through the transport of nutrients, phytoplankton and fish larvae, and to the distribution of geochemical tracers such as tritium, oxygen, chlorofluorocarbons and ^{14}C.

In addition, it is closely linked to the disposal of industrial wastes and the dispersion of various pollutants, which is the motivation of the present study.

In these regards, not a few works, either observational or theoretical, have been done for understanding to what extent the eddy-induced dispersion affects physical, chemical and biological processes in the mid-ocean (for instance, HAIDVOGEL *et al.*, 1983).

* Received March 1, 1993
** School of Environmental Sciences, University of Tsukuba, Tsukuba, Ibaraki-ken 305 Japan
*** Present affiliation: NTT Data Communications Systems Corporation, Toranomon, Tokyo 105 Japan

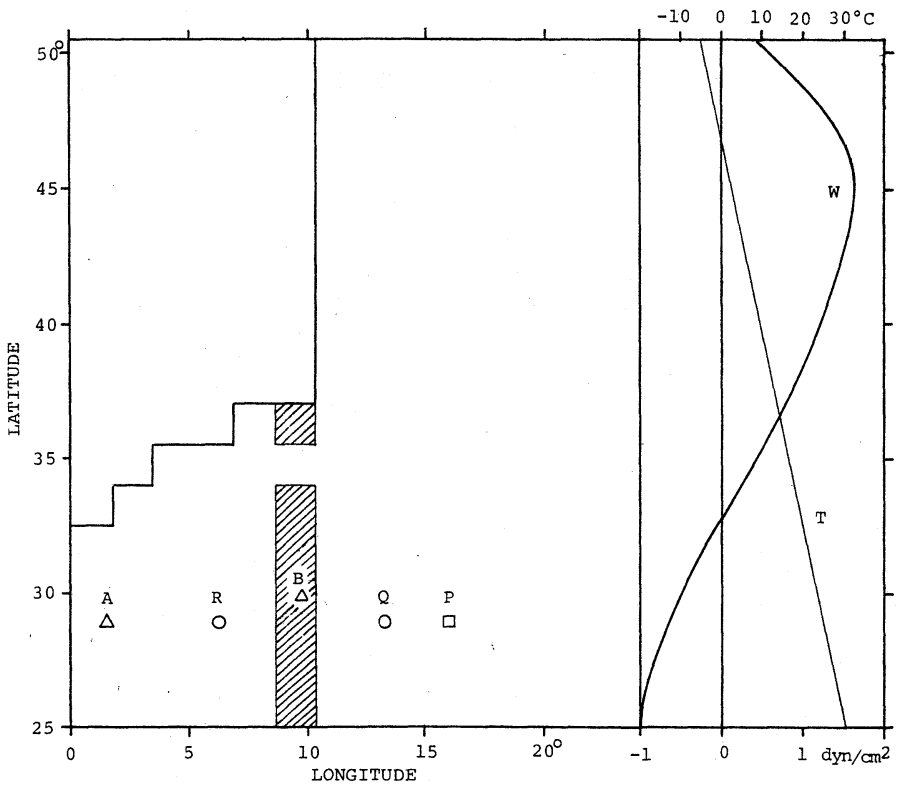

Fig. 1. Geometry of the ocean basin, wind stress (W) and reference atmospheric temperature (T). A ridge with a gap is shaded. A point source is located at P. Stick diagrams will be shown at Points A and B, and power spectra at Q and R.

However, our understanding still remains poor. The present study is concerned with dispersion of dynamically passive tracers, as a part of a preoperational survey of an area at 30°N, 147°E for ocean bottom disposal of radioactive wastes planned by Science and Technology Agency of Japan. A finite difference advection-diffusion equation for the tracers, initially distributed to the whole ocean surface and to a limited area on the ocean floor, is solved in a model ocean. The velocity field is supplied from a prognostic, four-level, eddy resolving ocean circulation model.

2. Eddy resolving circulation model

Quality of the numerical experiments on the tracer dispersion depends on the quality of the mesoscale eddy field to be used, which in turn depends on the eddy resolving ocean circulation model. Therefore, the ocean circulation model is briefly described first. The model ocean extends over 24.8° in longitude and from 25°N to 50.5°N in latitude as shown in Fig.1. The grid size is 0.43° in longitude and 0.375° in latitude. Four levels are set up in the vertical; the horizontal components of velocity, temperature and pressure are defined at depths of 80, 400, 1600 and 2600m, and the vertical component of velocity is defined at depths of 240, 1000 and 2100m. The bottom is 4000m deep except at a ridge the top of which is 2100m deep. A narrow gap 1.5° wide in latitude divides the ridge into a northern and southern branch. The ocean geometry is somewhat similar to a portion of the western North Pacific Ocean.

The conventional Laplacian form is used for the subgrid scale diffusion of momentum and heat. The salinity is made constant (35‰) everywhere. The density is calculated by a formula of FRIEDRICH and LEVITUS (1972).

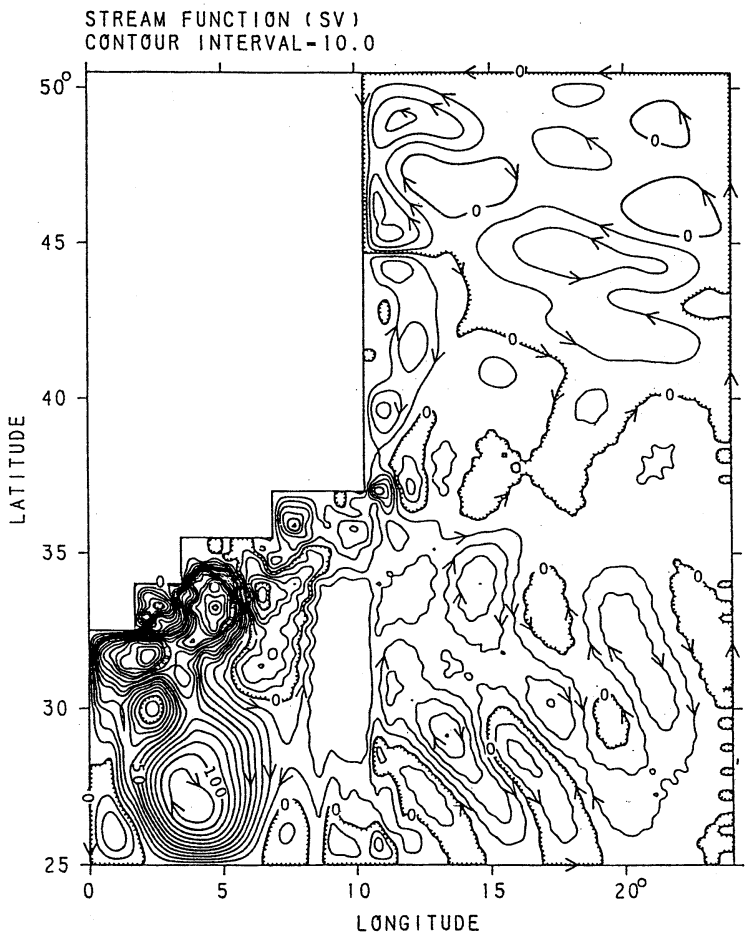

Fig. 2. A snapshot of the transport in terms of stream lines (units: Sv).

The circulation is driven by a prescribed wind stress and a prescribed reference atmospheric temperature shown in Fig.1. The wind stress has no meridional component. The surface heat flux is made proportional to the difference between the predicted surface temperature and the reference atmospheric temperature. The constant of proportionality is assumed to be 21W/m^2K (=50cal/cm^2 s K). There is no friction along the lower and lateral boundary. The vertical component of velocity vanishes at the surface (rigid-lid approximation). There is no heat flux across the lateral and lower boundary.

The finite differencing scheme is the same as that described in previous papers (TAKANO, 1974; Atomic Energy Management Center, 1986).

The coefficient of subgrid scale diffusion is $10^2 m^2/s$ for momentum and $10^3 m^2/s$ for heat. The coefficient of vertical diffusion is $10^{-4} m^2/s$ for momentum and heat. The time step is 30min.

In the initial state, the temperature is a function of depth and latitude only, the planetary vorticity advection for the barotropic component of velocity is balanced with the specified wind stress curl, and the shear current (baroclinic component of velocity) is determined from the given temperature distribution. Time integration is forwarded for about 230 years. For the last 80 years, the three components of velocity and temperature are saved every 2.5 days for analysis. The average temperature change rate is -2.1×10^{-3}°C/year if the

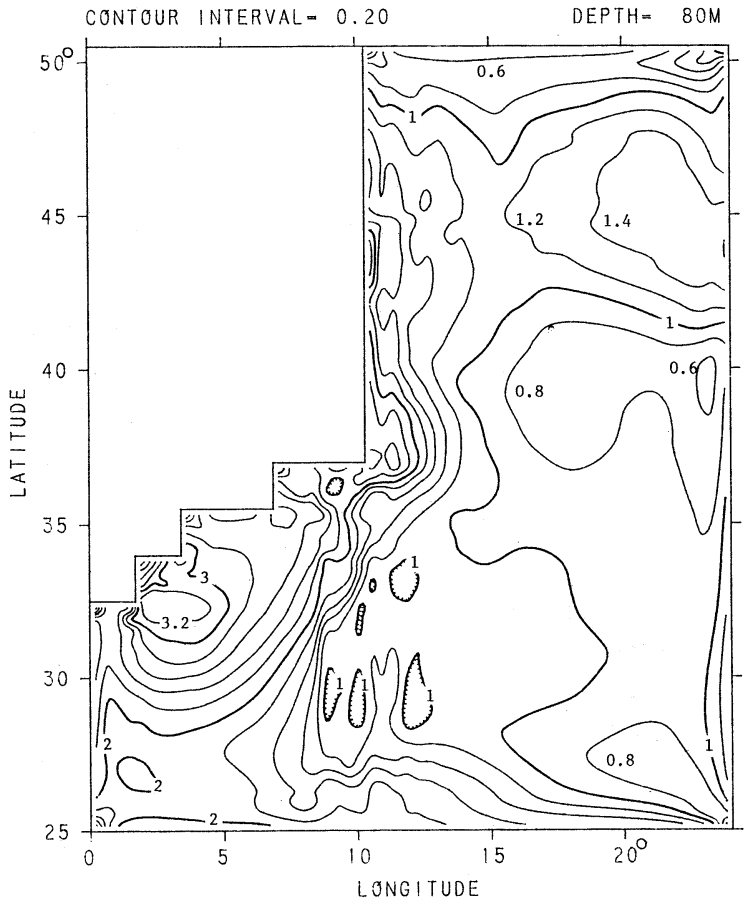

Fig. 3. Distribution of logarithms to the base ten of eddy kinetic energy (erg/cm^3) at a depth of 80m.

surface heat flux is calculated from the reference atmospheric temperature and surface temperature averaged over these 80 years, and then divided by the total water mass.

As a measure of the performance of the ocean model used here, Fig.2 shows a snapshot of the volume transport (vertical integral of the horizontal velocity from the bottom to the surface) in terms of the stream function. Mesoscale eddies are pronounced in and near the western boundary current flowing northeastward, while they are weaker in regions far apart from the western boundry current and on the ridge. There are, on the time-average (not shown), a subtropical gyre which transports 101Sv and a subarctic gyre which transports 41 Sv, but both gyres are veiled in strong mesoscale eddies in the snapshot.

Eddy activity distribution is described in Figs. 3 and 4 showing logarithms to the base ten of the eddy kinetic energy (erg/cm^3) at depths of 80 m and 2600 m. The maximum energy is found around 32.5°N, 3°E at both depths. It is four times greater at 80m than at 2600 m depth.

The mean kinetic energy is of almost the same order of magnitude as the eddy kinetic energy at a depth of 80m, but more than five orders of magnitude less in the greater part of the ocean basin at a depth of 2600 m except at the western boundary region where it is slightly less than the eddy kinetic energy.

Figure 5 gives examples of the velocity fluctuations in stick diagrams of the barotropic and baroclinic components of velocity at points A and B in Fig.1 for a period of 2580 days arbitrarily chosen. The deviations from the time-

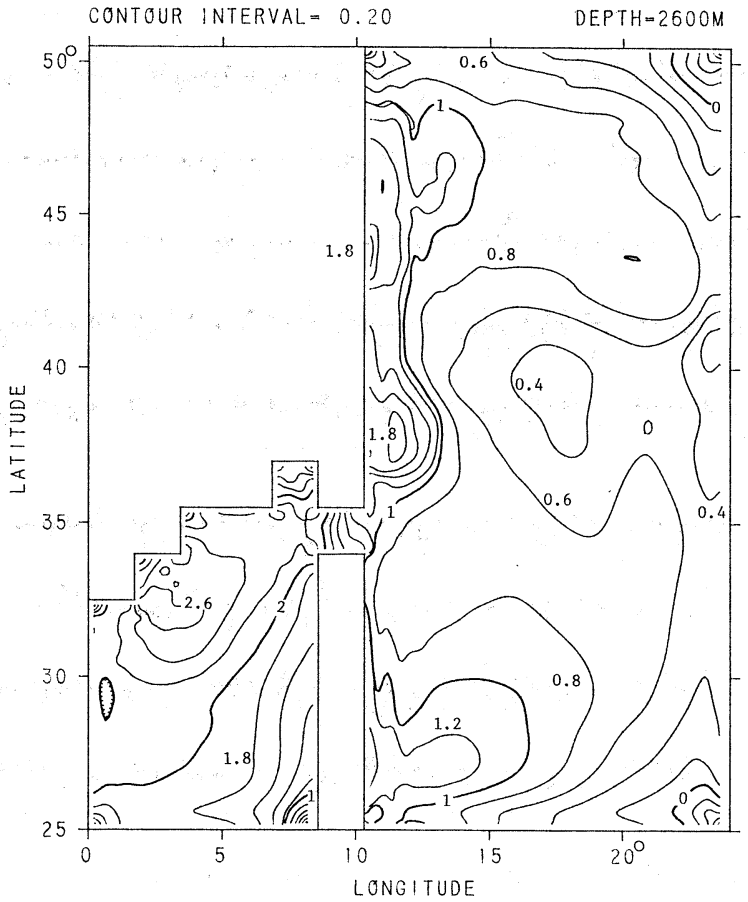

Fig. 4. Same as Fig. 3 except for a depth of 2600m.

average are shown. The average eastward and norhward barotropic components are −3.7 cm/s, −1.1 cm/s at A, and 0.073 cm/s, −1.4 cm/s at B, which are much smaller than the deviations. At A, the average eastward and northward baroclinic components of velocity are −0.96 cm/s, 3.6 cm/s at 80 m depth, −1.0 cm/s, 1.7 cm/s at 400 m depth, −0.17cm/s, −0.29 cm/s at 1600 m depth, 0.62 cm/s, −0.95 cm/s at 2600 m depth; at B, 3.8 cm/s, 1.3 cm/s at 80 m depth, 0.10 cm/s, 0.40 cm/s at 400 m depth, −0.90 cm/s, −0.55 cm/s at 1600 m depth, which are also much smaller than the deviations. Fluctuations of periods of about 100 days are apparent. The deviations of the barotropic com-ponent are much larger than those of the baroclinic components at most grid points throughout this period and any other period, but the formers are comparable with the latters at 400m depth at B.

The baroclinic components are well correlated between 80m and 400m depths. It is also the case between 1600m and 2600m, but the correlation is poor between 400m and 1600m depths. The barotropic components is correlated with the baroclinic components at 80m and 400m depths rather than at 1600m and 2600m depths.

Figure 6 shows stream lines for the meridional circulation calculated from the meridional and vertical component of velocity integrated over the parallel of latitude. If the velocity components are integrated, there appears no deep downwelling reaching to the bottom in high latitudes. Moreover, reflecting the limited size of the ocean basin, the meridional circulation is rather weak: the downward transport at high

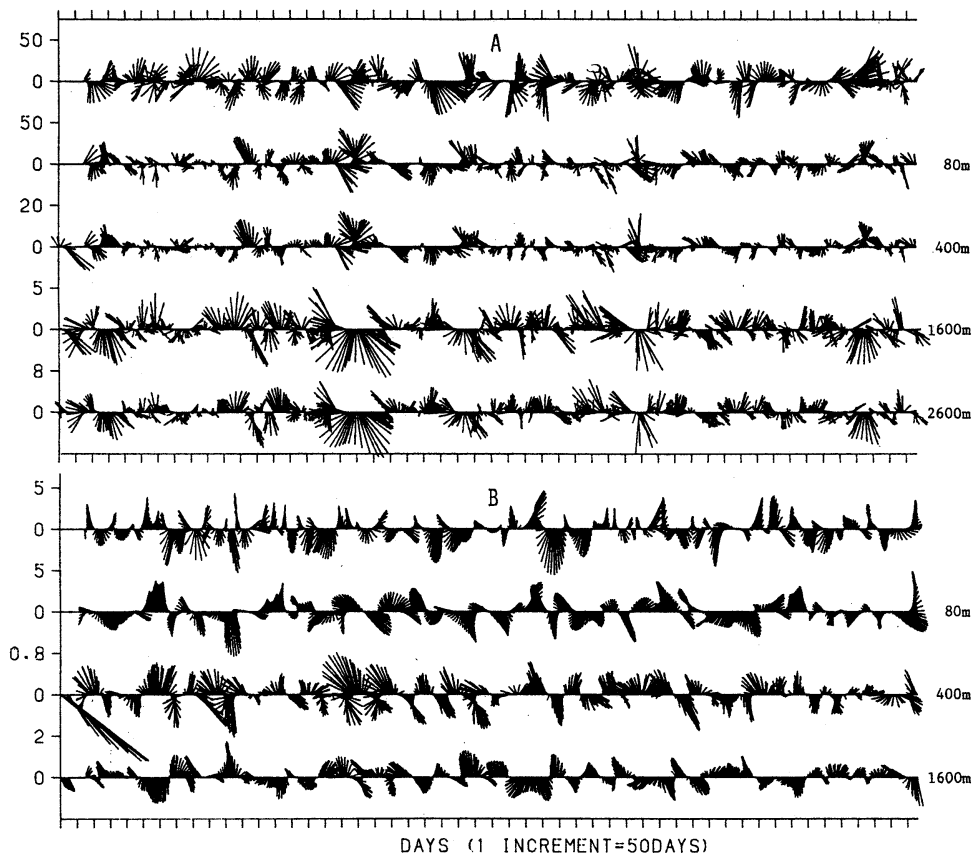

Fig. 5. Stick diagrams at Points A (upper panel) and B (lower panel). The top diagram of each panel is the deviation of the barotropic component from its time-average. The lower diagrams are the deviations of the baroclinic components from their time-averages. One increment in abscissa is 50 days. The scale in ordinate (cm/s) is variable.

latitudes is only 5 Sv. As to the velocity itself, the deviation from the time-average is much stronger than the time-average in most grid points, but the average meridional circulation calculated from the deviation is weak compared with that calculated from the time-average, because the effect of mesoscale eddies is almost canceled each other if integrated over the parallel of latitude.

Power spectra of the eastward and northward components of velocity are shown in Figs.7 and 8 at two points Q and R (Fig.1) arbitrarily chosen. Clearly appear mesoscale fluctuations of periods of some hundreds of days. For comparison, power spectra are calculated (not shown here) from observed 7-year current velocity data at a depth of 5000m at 30°N, 147°E (IMAWAKI and TAKANO, 1982), which was done also in the framework of the preoperational survey for ocean bottom disposal of radioactive wastes. Although the numerical simulation is successful in generating mesoscale fluctuations, energy decay in high frequencies is much sharper than that with the observed data. This sharp decay in the simulation could be attributed to neglect of the tidal currents and to a grid size of about 40 km which is too coarse to resolve small scale motions in high frequencies. Because the shortest resolvable wavelength is two times the grid size, the model cannot resolve fluctuations of wavelengths shorter than 80km, so that the kinetic energy in higher frequencies is more or less

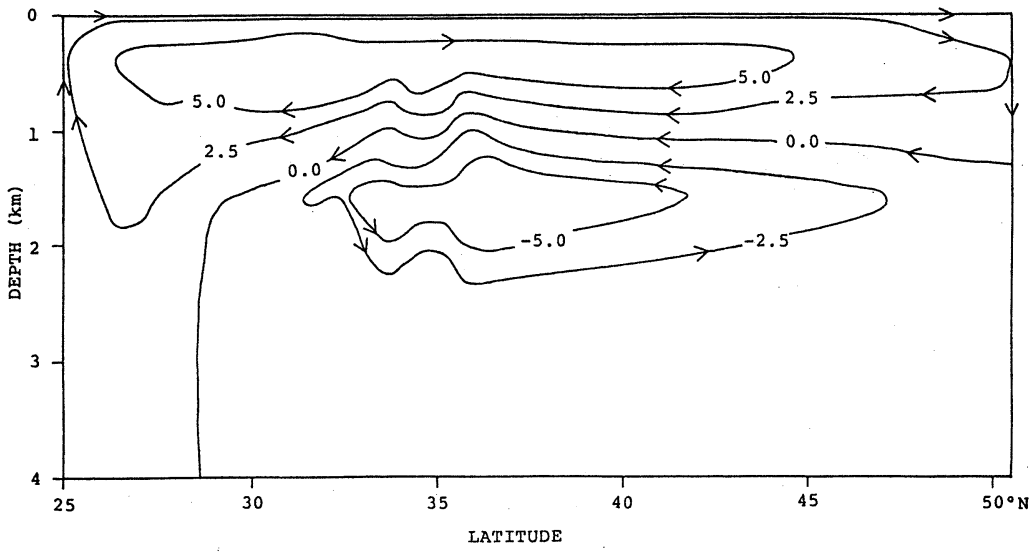

Fig. 6. Steam lines for the time-average of the meridional circulation (units: Sv)

cut off. Inertia oscillations are not resolved, either; their scales are too small. In short, the simulated velocity field is simpler than the observed one.

3. Numerical experiments on large scale dispersion

An advection-diffusion equation for concentration C of any dynamically passive tracer is solved as an initial-boundary value problem. The conventional Laplacian form is used for the subgrid scale diffusion. The coefficient of horizontal diffusion is $10^3 m^2/s$. The coefficient of vertical diffusion is $10^{-4} m^2/s$. A much more scale selective biharmoic formulation is useful for suppressing computational noise arising from advection and diffusion terms (YOKOYAMA and TAKANO, 1986), but is put aside on account of complicated finite difference analog of the lateral boundary condition.

Although the centered differncing (leap-frog) scheme is used basically for time integration, the Euler-Matsuno backward differencing scheme is used every ten time steps for suppressing computational noise and separation of the solutions. The centered differencing scheme is also used for space differencing except for both horizontal and vertical advection, which are calculated by the upcurrent scheme.

The velocity field is supplied from the ocean circulation model described above. Since the velocity data are available at intervals of 2.5 days, the velocity field at a given time necessary to time integration is calculated by linear interpolation of the two nearest data.

An additional term $-\alpha C$ appears in the equation if a radioactive substance with decay constant α is dealt with. However, the solution with $\alpha = 0$ also holds good for a radioactive substance provided that it is multiplied by a factor of $\exp(-\alpha t)$ (t: time), so that α is put as 0 in the present study.

Two cases are studied; dispersion from the surface (Case 1), and dispersion from the bottom (Case 2). In Case 1, a concentration of 50 in arbitrary units is uniformly given, as an initial condition, to each of all the grid points at the surface layer 240m thick. In Case 2, a concentration of 5000 in arbitrary units is given to Point P in Fig.1 at the bottom layer 1900m thick as an initial condition. The location of point P in Fig.1 might correspond with the location of a proposed area for the ocean bottom disposal of low-level radioactive wastes at 30° N, 147° E, about 400km east of the Izu-Ogasawara Ridge and about 500km south of the Kuroshio Extension. In both cases, there is no flux of C across the lateral, upper and lower boundaries.

Since the primary objective is to understand the effet of the mesoscale eddies, two runs are

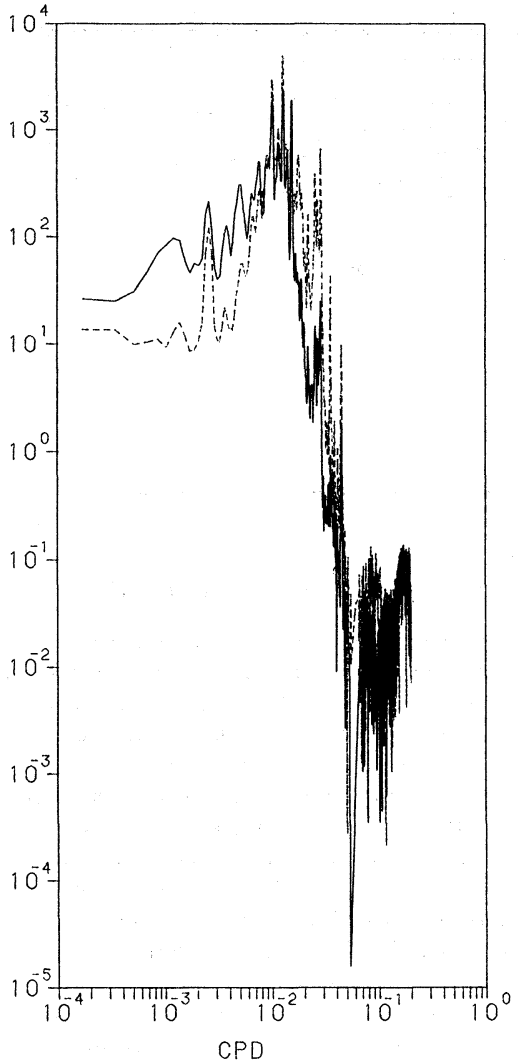

Fig. 7 Power spectra of the eastward (full line) and northward (broken line) components of velocity at 2600m depth at Point Q.

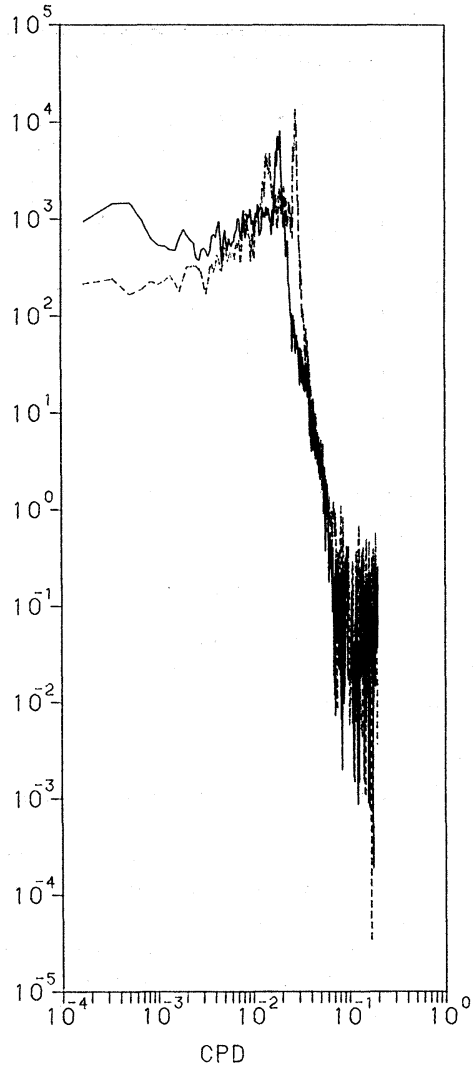

Fig. 8. Same as Fig.7 except for Point R.

achieved in each case; one is by using the velocity field comprising mesoscale eddies and the other by using the velocity field averaged over 80 years. Hereafter, the former is referred to as Case 1e and Case 2e, and the latter as Case 1a and Case 2a.

Time integration is forwarded by a time step of 1.5 hours in Cases 1e and 2e, and a time step of 2 hours in Cases 1a and 2a until a steady state is reached where the initially given substance is completely dispersed and its concentration becomes constant in space and time. Theoretically, this constant is 3.06 in Case 1 and 0.936 in Case 2, because the total amount of C, 5.43 $\times 10^7$ units in Case 1 and 1.66×10^7 units in Case 2, is initially given into a total water volume of $1.77 \times 10^7 km^3$. However, the value finally reached by time integration is 3.02 in Case 1e, 2.98 in Case 1a, 0.923 in Case 2e and 0.918 in Case 2a. The small discrepancies between these values and theoretical values (3.06 or 0.936) result from loss of C due to round-off and truncation in the course of time integration, which usually happens to such calculations on the computer.

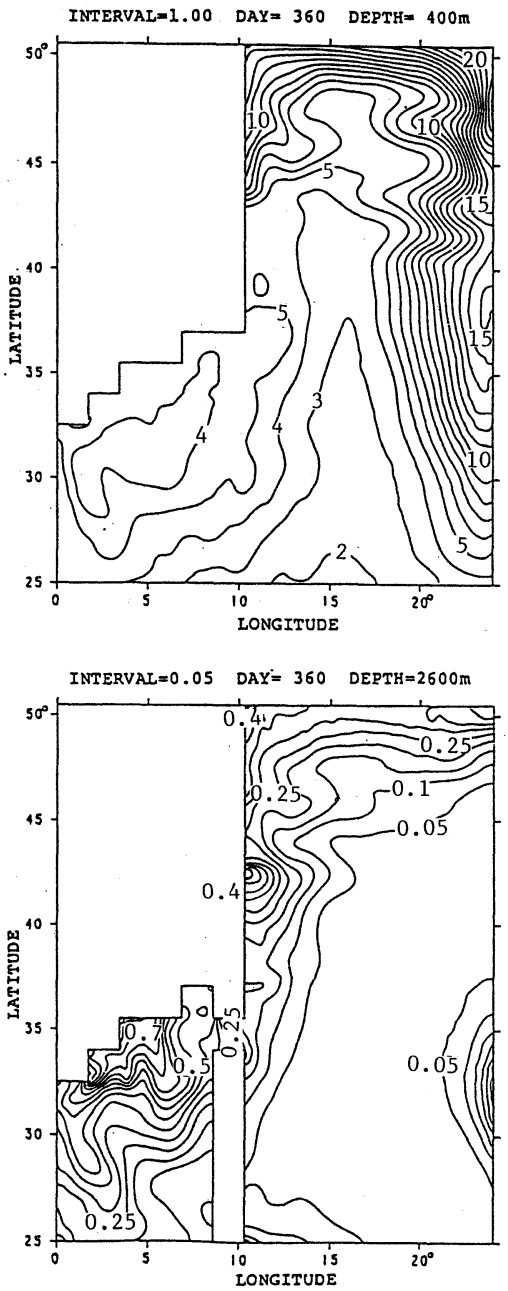

Fig. 9. Isopleths at depths of 400m and 2600m at day 360 in Case 1e.

4. Dispersion from the surface

4.1 Case 1e

Figure 9 shows isopleths of C at depths of 400m and 2600m at day 360 after setting in dispersion. Due to a strong sinking of surface water near the northern boundary, the concentration in lower layers increases first in the northern part of the basin and then disperses southward. At the surface, there are a convergence region near the western boundary around 42°N and another broad convergence region near the eastern boundary around 41°N, which are also sources of C for the lower layers, though not so strong as near the northern boundary. Isopleths at 400m depth do not suggest the presence of the ridge.

The averages over the parallel of latitude at days 360, 720 and 1440 are shown in Fig. 10. Near the northern boundary, there is a downward dispersion associated with a strong sinking. In the other surface regions there is no such a strong downward dispersion, which leads to a sharp vertical gradient of C between the surface layer and the underlying layer, in particular, in the southern region at the early stages (days 360 and 720). These features qualitatively agree with an observed distribution of anthropogenic tritium penetrating into deep waters (OSTLUND and BRESCHER, 1982). The sharp vertical gradient almost vanishes at day 1440, though the southward dispersion from the northern region is still persistent. Small spikes and a dome rising from the bottom in the isopleths at day 1440 are fictitious due to peculiarities of the computer plotting program.

The gap 1.5° wide in latitute of the ridge is not an effective pathway from the east to the west of the ridge in the bottom layer; the tracer sinking to lower layers from the northern boundary region and the surface convergence areas at the eastern boundary region at about 41°N and at the western boundary region does not come to the west of the ridge through the gap. In the bottom layer west of the ridge, C increases due to sinking from the upper layers where C is transported from the central and eastern regions by the subtropical gyre. Then, C at a depth of 2600m is higher on the western side than on the eastern side of the ridge.

Mesoscale fluctuations of isopleths due to the mesoscale eddies are seen throughout time integration until a steady state is reached.

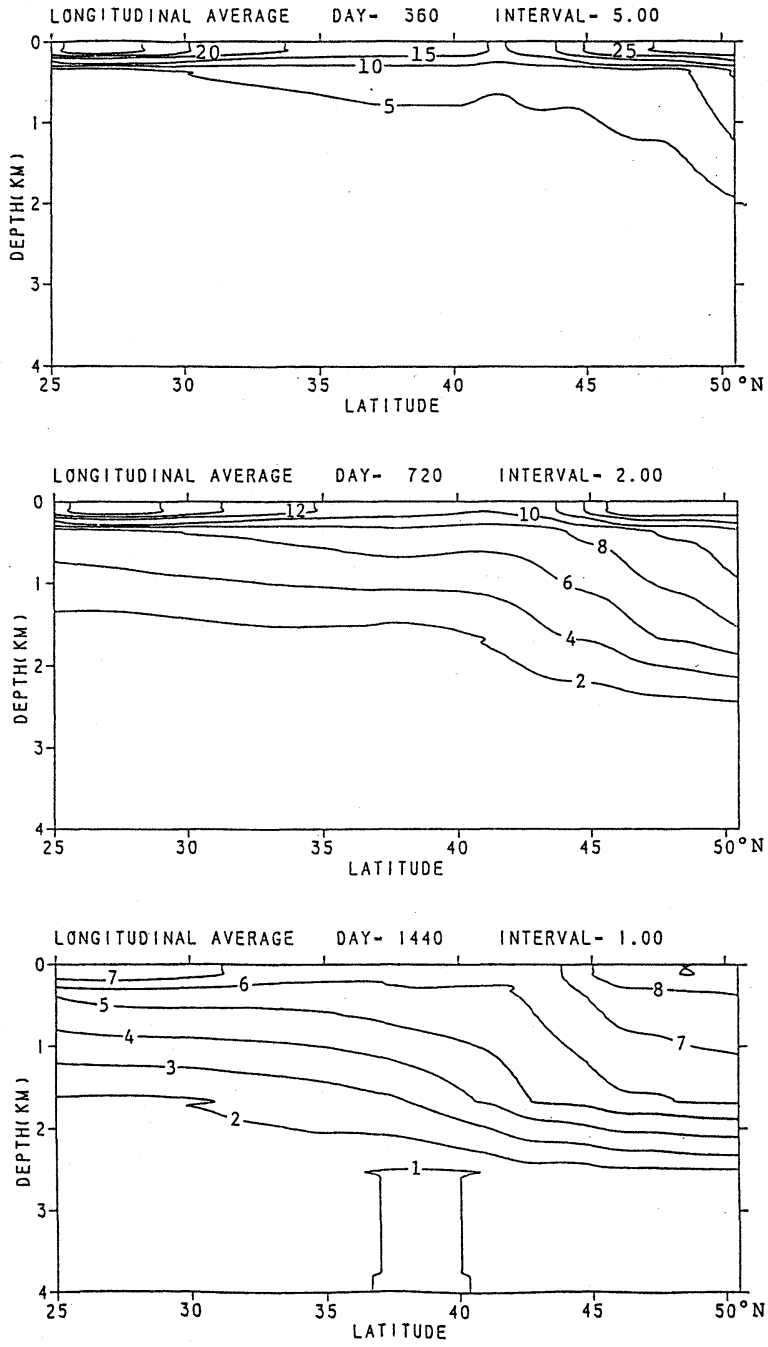

Fig. 10. Vertical-latitude distribution at days 360 (top), 720 (middle) and 1440 (bottom) in Case 1e.

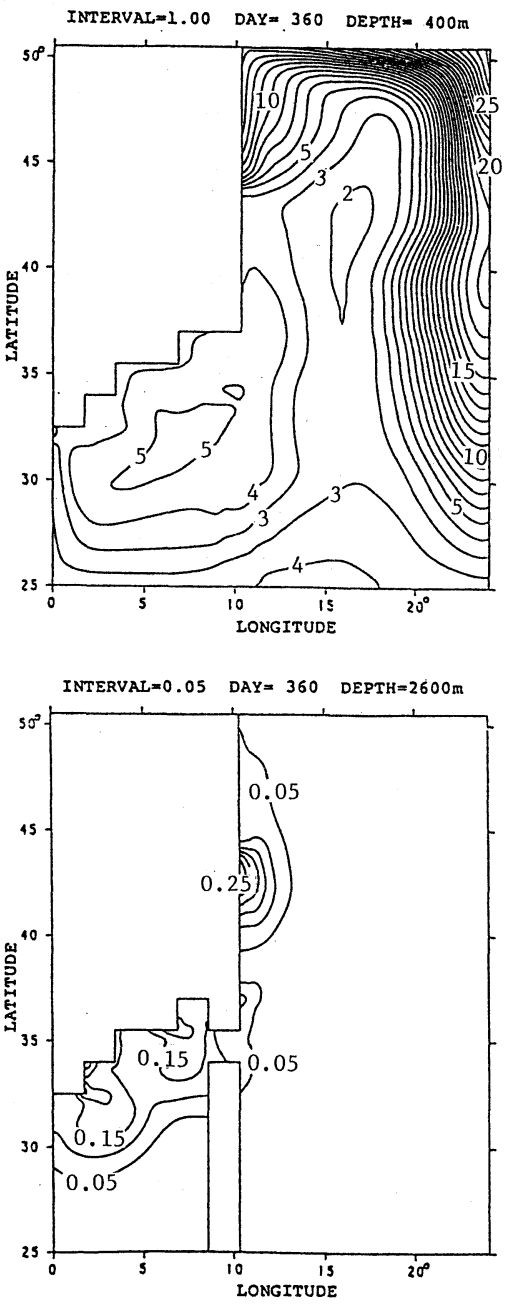

Fig. 11. Isopleths at depths of 400m and 2600m at day 360 in Case 1a.

4.2 case 1a

In this case, the advection is calculated with the time-average velocity field. Figure 11 shows isopleths at depths of 400m and 2600m at day 360. The isopleths become smoother without mesoscale eddies. Although the principal features of dispersion at 400m are similar to those in Case 1e, the concentration is higher, particularly near the northeastern corner and most of the eastern boundary areas, except in most areas between about 35° N and 45° N. At a depth of 2600m, the concentraion is everywhere lower than in Case 1e.

At a depth of 80m, the concentration near the northern boundary is about 34 in Case 1e and about 40 in Case 1a. Near the southern boundary, it is about 27 in Case 1e and about 37 in Case 1a, which indicates slower downward dispersion from the surface in Case 1a because of absence of mesoscale eddies. In the northern boundary region at a depth of 400m, the amount of C coming from the surface is smaller in Case 1a than in Case 1e, but the downward and southward dispersion from there are not strong, so that C stagnates to be higher than in Case 1e. This point will be again discussed later.

Figure 12 shows the average over the parallel of latitude at days 360, 720 and 1439. There is qualitatively no significant difference between Cases 1a and 1e (Fig.10), but the concentration at the surface layer is higher in Case 1a because of slower downward despersion.

5. Dispersion from the bottom

A concentration of 5000 in arbitrary units is initially given to the bottom layer at P, i. e., to a vertical pillar 1900m high of which the trapezoidal horizontal section is 41.7km in meridional side length and 41.9km in mean zonal side length.

5.1 Case 2e

At day 360 no dispersed substance practically reaches to the surface layer. The maximum surface concentration appears off the western coast from 33° N to 37° N, but is less than 0.01. Due to westward currents in the subtropical gyre at the upper two layers, the westward dispersion is more prominent than the northward dispersion at depths of 400m and 1600m (not shown here).

At day 720 the maximum surface concentration reaches to 0.19 at a coastal point (34° N, 1.92° E) and the maximum concentration at the bottom layer decreases to 5.5 which is located near Point P. The maximum concentration is

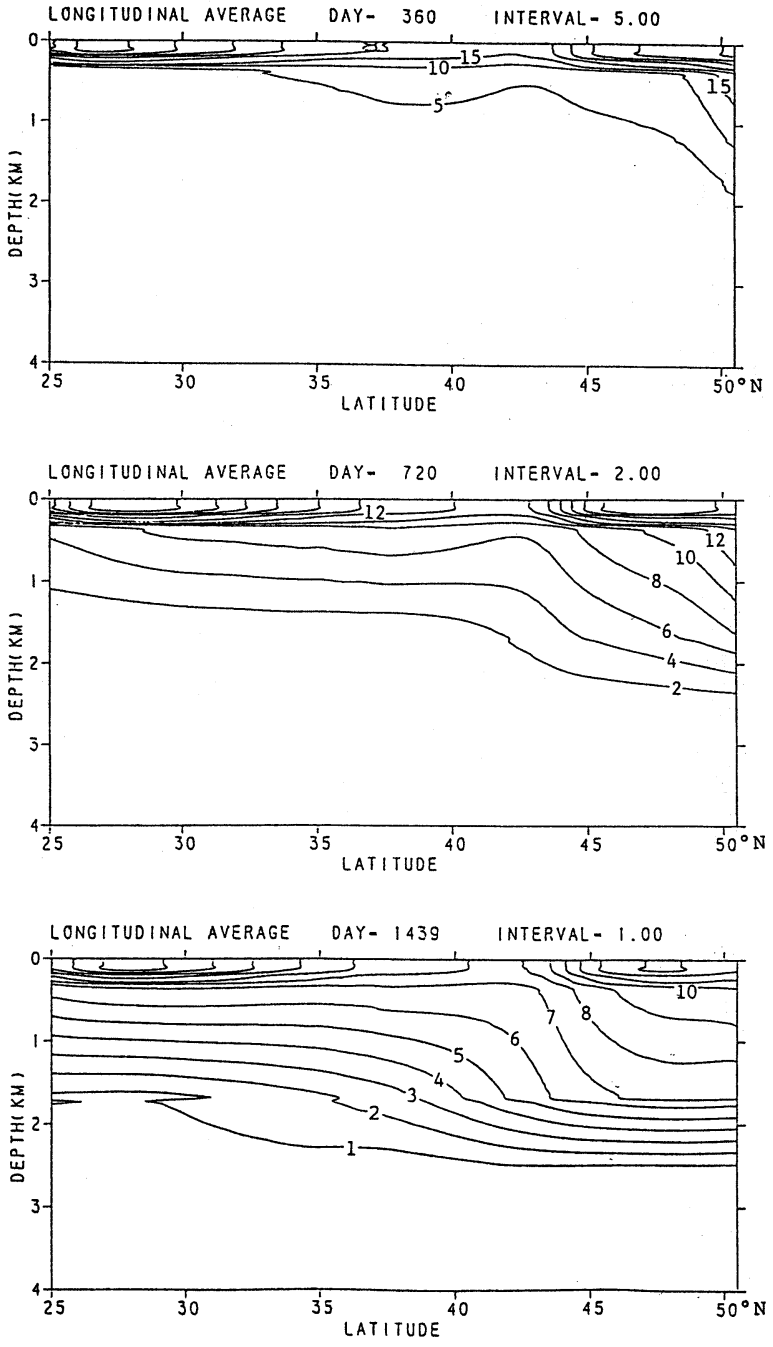

Fig. 12. Vertical-latitude distribution at days 360 (top), 720 (middle) and 1440m (bottom) in Case 1a.

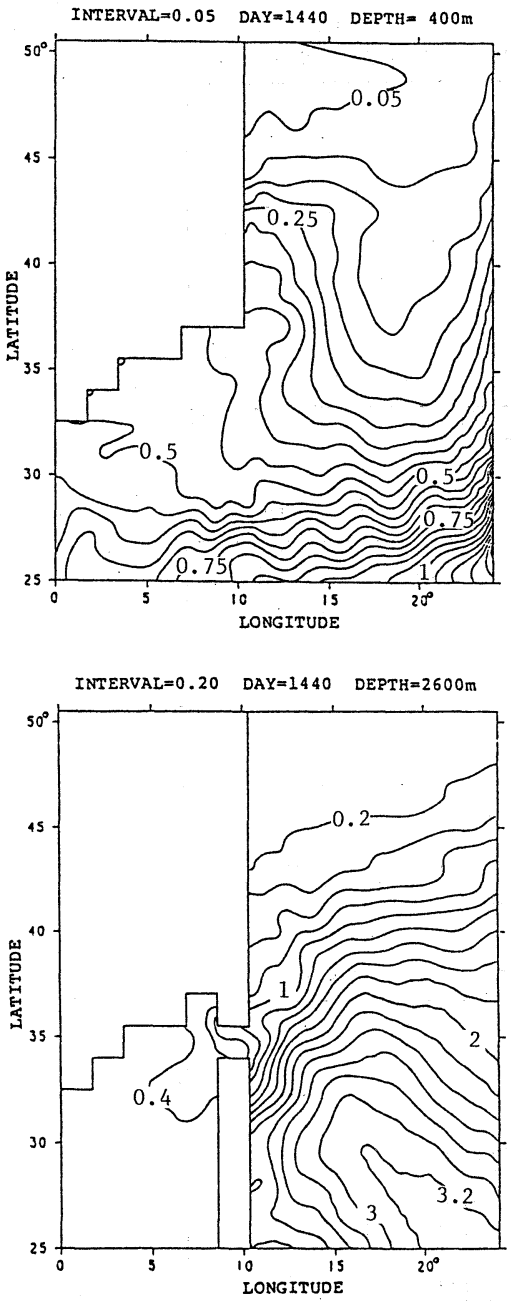

Fig. 13. Isopleths at depths of 400m and 1600m at day 1440 in Case 2e.

3.05 at a depth of 1600m. It is located at 26°N, 20°E, southeast of P. At a depth of 400m, it appears far east, at the southeastern corner. The pattern of isopleths at each layer is not very different from that at day 1440 shown in Fig.13.

The distribution at day 1440 shows that the ridge almost blocks the westward dispersion in the bottom layer. Because there is no strong sinking along the western side of the ridge, dispersion into the deep layer west of the ridge takes place only through a gap between the northern and southern branches of the ridge, but the gap is not an effective pathway.

The maximum concentration is not seen at the location of P anymore at a depth of 2600m, but it is at the southeastern corner at depths of 400m, 1600m and 2600m, and near the western coast at a depth of 80m as at day 720.

Figure 14 shows the longitudinal average at days 360, 720 and 1440. Upwellling in low latitudes gives rise to the upward dispersion from the bottom source. Then, northward flows in upper layers, particularly in the western boundary region, give rise to the northward dispersion. In addition to this pathway, a direct northward pathway is effective in the bottom layer.

5.2 Case 2a

At day 720, the maximum concentration is 9.0 at a depth of 2600m and 1.15 at a depth of 1600m, 0.18 at a depth of 400m and 0.05 at a depth of 80m to be compared with 5.5, 3.05, 0.84 and 0.18, respectively, in Case 2e. Because the upward dispersion is slower in Case 2a, the concentration remains higher in the source region, and lower in the upper layers.

Figure 15 shows isopleths at day 1440. Although the isopleths are smooth, free from mesoscale fluctuations compared with Case 2e, the general pattern of them are similar to each other except at the source region at the bottom layer. Isopleths are mostly closed curves in Case 2a, but not so in Case 2e. The maximum concentration is 4.8 at 2600m, 1.5 at 1600m, 0.45 at 400m and 0.16 at 80m to be compared with 3.2, 2.7, 1.2 and 0.46, respectively, in Case 2e. This confirms slower upward dispersion than in Case 2e. Figure 16 shows the average over the parallel of latitude at days 360, 720 and 1440. Comparison with Case 2e (Fig.14) shows that the mesoscale eddies enhance the vertical dispersion rather than the horizontal dispersion. Slow upward dispersion in Case 2a brings about a sharper vertical gradient of concentration

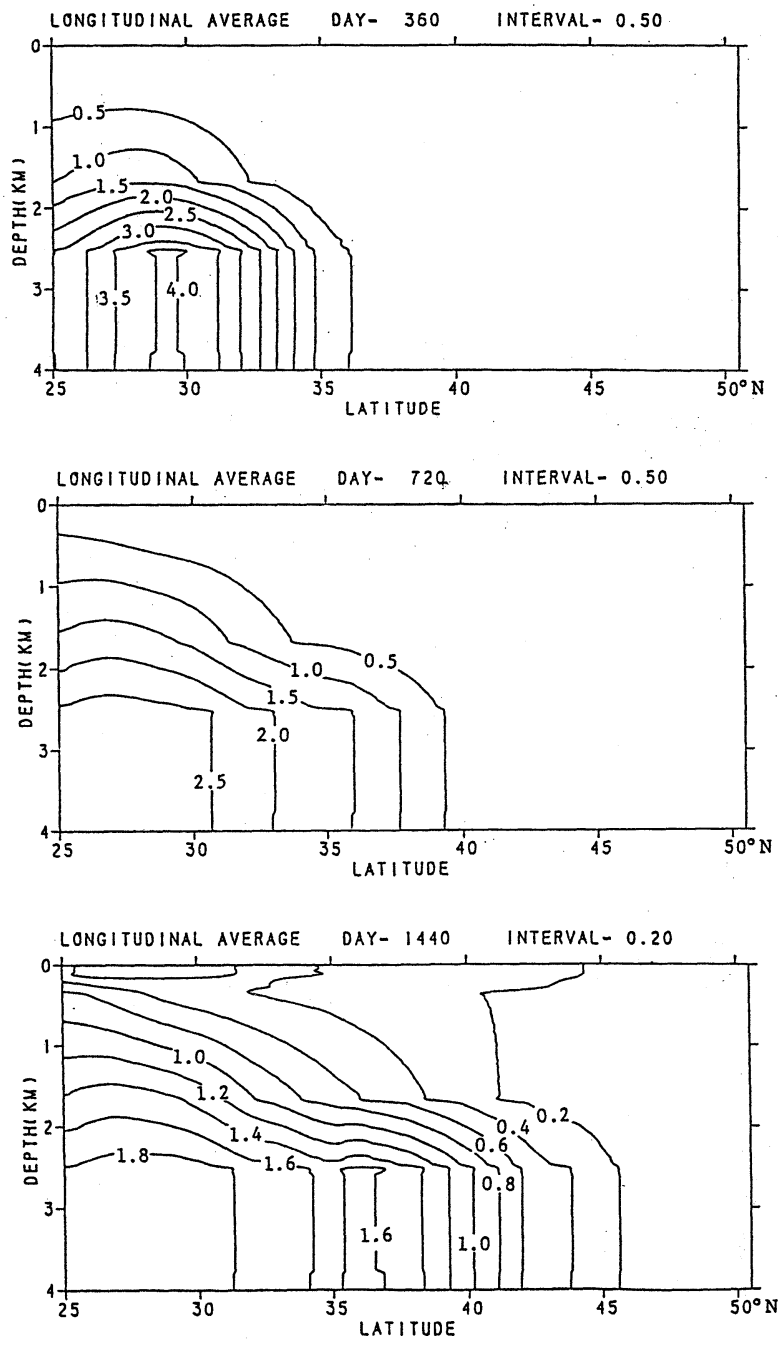

Fig. 14. Vertical-latitude distribution at days 360 (top), 720 (middle) and 1440 (bottom) in Case 2e.

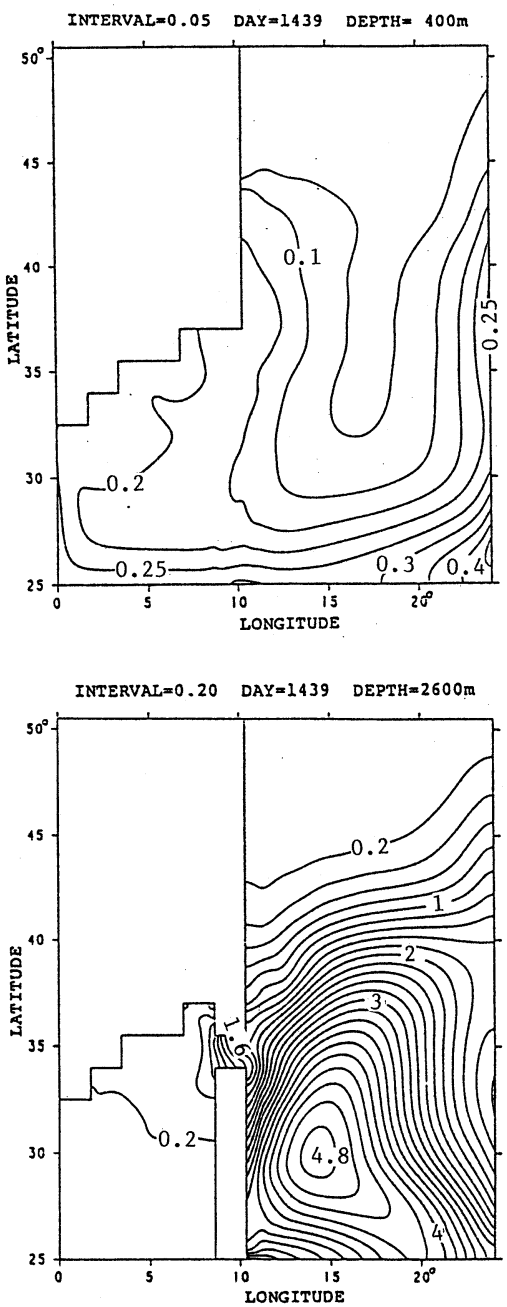

Fig. 15. Isopleths at depths of 400m and 2600m at day 1440 in Case 2a.

between the bottom and upper layers than in Case 2e.

6. Layer-average downward and upward dispersion

The downward dispersion in Cases 1e and 1a is shown in Figs.17 and 18 in terms of the average and total amount of C in each layer. Layer 1, the uppermost layer, is 240m thick, layer 2 is 760m thick, layer 3 is 1100m thick and layer 4 is 1900m thick. In both cases, the average and the total amout in the surface layer monotonically decrease with time and those in the bottom layer monotonically increase with time, whereas those in layers 2 and 3 first increase and then decrease with time. This implies that C becomes excessive in a sense in thin layers 2 and 3 in a transition stage before the dispersion into the thick bottom layer is fully developed.

Apparently the final steady state is reached in shorter time in Case 1e than in Case 1a. Table 1 tabulates the time required for the average concentration in each layer to reach 95 or 105% of the final uniform value (3.02 in Case 1e and 2.98 in Case 1a), and the ratio of the time in Case 1a to that in Case 1e. The mean ratio 2.11 confirms the striking effect of the mesoscale eddies.

Figures 19 and 20 show the upward dispersion in Cases 2e and 2a in the same way. In both cases, both average and total amount in each of the three upper layers monotonically increase with time. Contrary to Cases 1e and 1a, there is no stagnation in layers 2 and 3, because the thickness of the layer decreases upward, the advection is stronger in the upper layers and the source is located in the bottom layer.

Table 2 gives the time required for the average of C to reach to 95 or 105% of the final value (0.923 in Case 2e and 0.918 in Case 2a), and the ratio of the time in Case 2a to that in Case 2e. The mean ratio is 1.85. In these cases, too, the time for the complete dispersion is reduced by about half by the effect of mesoscale eddies.

It takes about 15 years in Cases 1e and 2e, and about 30 years in Cases 1a and 2a to reach the almost complete dispersion where the concentration ranges between 95 and 105% of the final value. The complete dispersion requires, however, about 30 years in the former cases and about 50 years in the latter cases as shown in Figs.17 to 20.

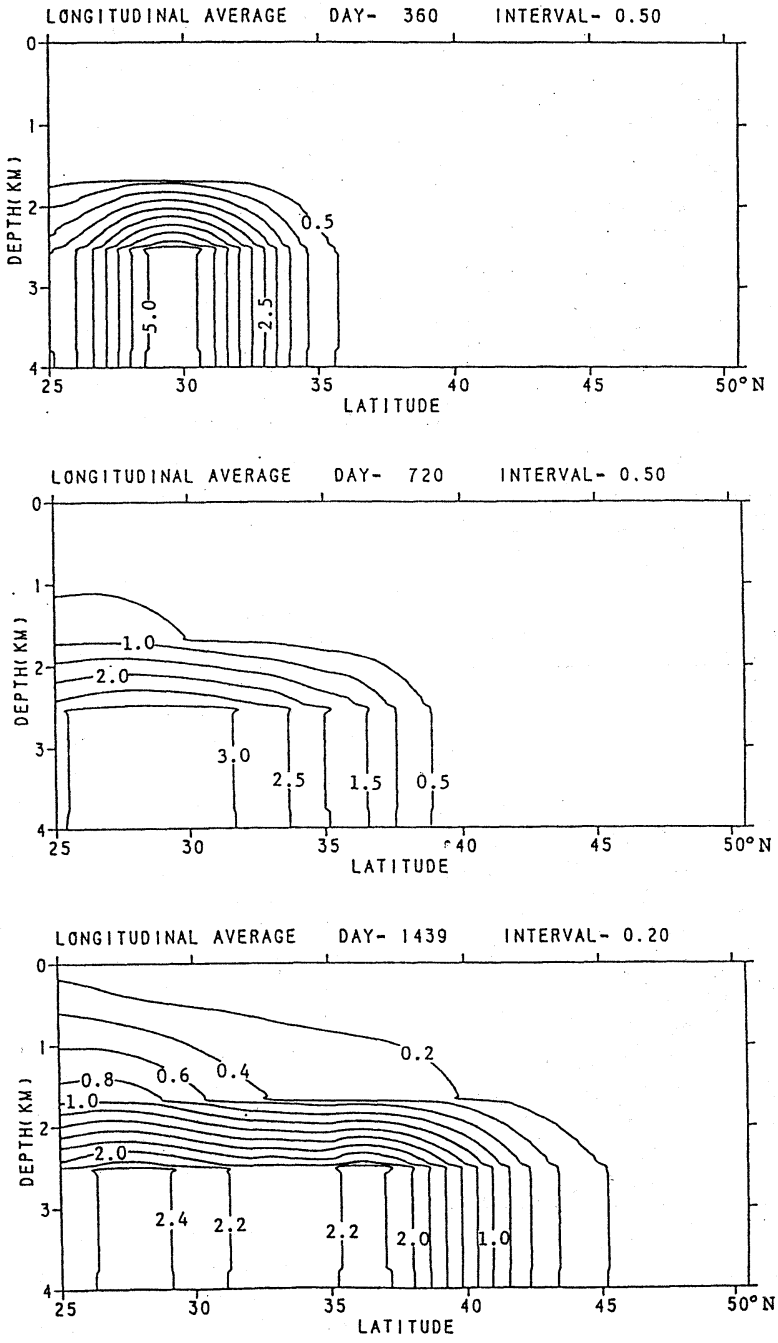

Fig. 16. Vertical-latitude distribution at days 360 (top), 720 (middle) and 1440m (bottom) in Case 2a.

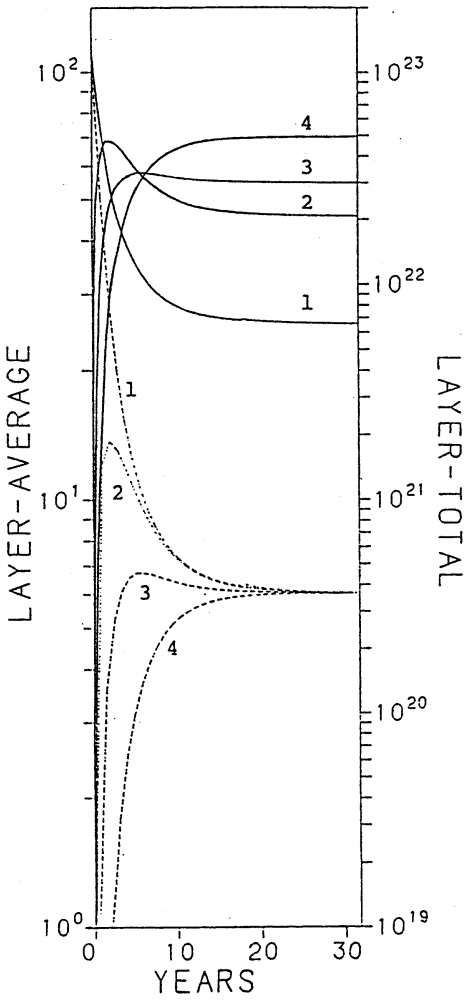

Fig. 17. Average and total amount of C in each layer as a function of time in Case 1e. Solid curve for the total amount, and broken curve for the average. Numerals alongside the curves refer to the layer numbers; 1 to the uppermost layer and 4 to the lowermost layer.

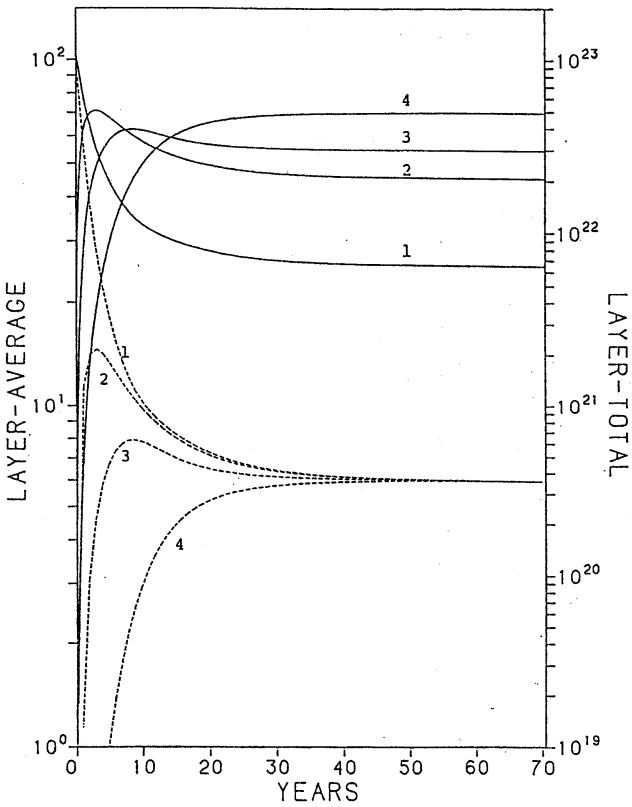

Fig. 18. Same as Fig.17 except for Case 1a.

7. Concluding remarks

The above results are summarized as follows.

(1) Tracers initially given to the whole surface of the model ocean are transported by the general circulation first northward in surface waters and then downward at high latitudes, which is in qualitative agreement with observations.

(2) Tracers initially given to a bottom area east of the meridional ridge are dispersed in both horizontal and vertical direction. Its westward dispersion in the bottom layer is obstructed by the ridge, while the isopleths of tracer concentration in upper layers west, above and east of the ridge do not seem to reflect the presence of the ridge. The mesoscale eddies enhance the vertical dispersion rather than the horizontal dispersion in the bottom layer. Although the discussion on the mesoscale eddies themselves is out of the scope of the present study, it might be remarked that, approaching the ridge, the mesoscale eddies do not shrink vertically to get over it.

(3) To reach the complete dispersion in both cases (downward dispersion from the surface source, and upward dispersion from the bottom source), it takes about 30 years in the mesoscale eddy field and about 50 years in the time-average field. The mesoscale eddies significantly enhance the dispersion over the whole ocean basin.

It might be parenthetically noted that, as to

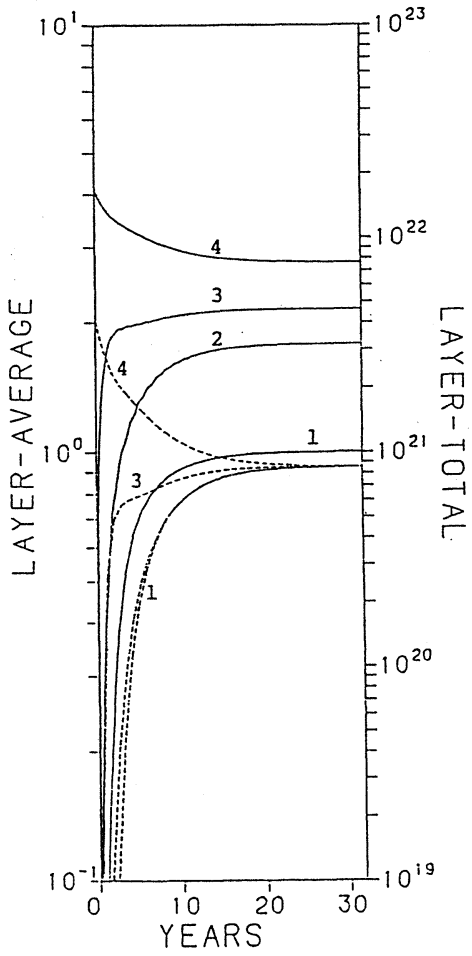

Fig. 19 Same as Fig. 17 except for Case 2e.

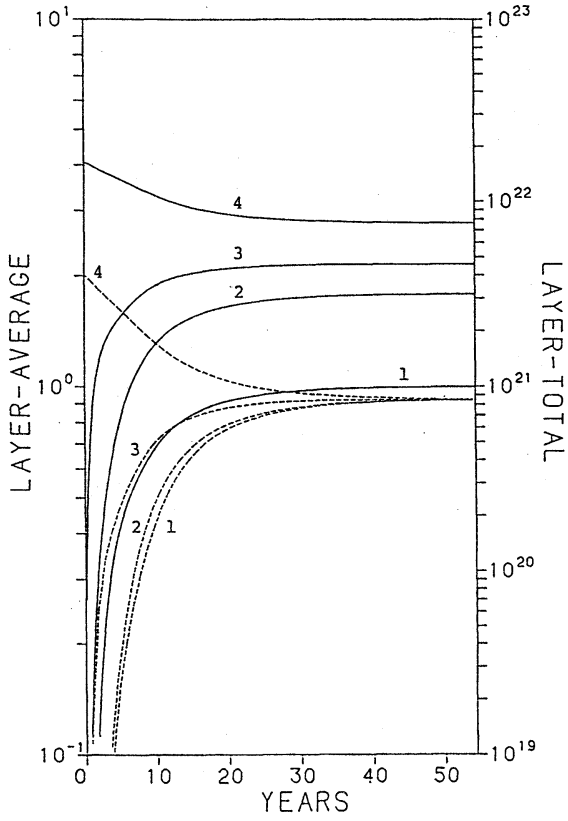

Fig. 20 Same as Fig. 17 except for Case 2a.

Table 1. Time (in years) required for the average concentration in each layer to reach to 95 or 105% of the final value in Case 1e (E) and 1a (A), and the ratio A/E.

Layer	1	2	3	4	mean
E (Case 1e)	16.4	15.9	11.0	13.4	
A (Case 1a)	34.7	33.5	25.0	26.0	
A/E	2.12	2.11	2.27	1.94	2.11

Table 2. Same as Table 1 except for Case 2e and Case 2a.

Layer	1	2	3	4	mean
E (Case 2e)	15.5	15.5	11.0	14.6	
A (Case 2a)	29.9	28.4	19.7	26.9	
A/E	1.93	1.83	1.79	1.84	1.85

dynamically active tracers, both horizontal and vertical heat transport are, if averaged over the vertical or horizontal cross-ocean section, little affected by mesoscale eddy activity (HAN, 1975; TAKANO, 1982).

A shortcoming of the present study is that the model ocean basin is very small; its volume is 1.77×10^7km^3, only 1.3% of the volume of the world ocean and 2.4% of the volume of the Pacific Ocean (72.4×10^7km^3). The time required for the complete dispersion in the model ocean is about 30 years (Figs.17 and 19), while the turnover time inferred from ^{14}C and others in the real ocean is a thousand of years or longer. The time scale of three-dimensional dispersion might be nearly proportional to the volume of the ocean basin, so that a period of 30 years in the model ocean should be equivalent to 2308 (=30/0.013) years for the world ocean and to 1250 (=30/0.024) years for the Pacific Ocean. These values, about 2300 and 1250 years, are reasonable compared with observations. This is somewhat surprising because the short longitudinal extent of the model ocean may increase the relative importance of the western boundary region where the eddy activity is high, which should turn out to exaggerate the eddy activity and eddy-induced dispersion in the small model ocean compared with the actual large ocean basin. As far as the eddy activity at point P in the simulation is compard with that by observed data, the eddy kinetic energy is at least one order of magnitude stronger than the observed one.

The poor vertical resolution is not capable of simulating the thermocline as sharply as observed, so that the vertical dispersion through the thermocline may not be correctly simulated. Therefore, the dispersion might be unrealistically strong in the numerical model. In addition, the bottom topography cannot be realistically set up, either.

A limited zonal extent of the model ocean might more or less distort high frequency, long Rossby waves, which affects the simulated mesoscale eddy properties.

In these regards, eddy resolving circulation models and dispersion models in larger ocean basins with finer vertical resolution are expected to run in the near future.

Other numerical experiments are carried out by using current velocities obtained with the non-slip condition instead of free-slip condition along the lateral boundary. The mesoscale eddy properties and tracer dispersion do almost not change.

The coefficients of subgrid scale diffusion are taken as small as possible, if large enough to suppress the computational noise and instabillity. The coefficients of eddy diffusion calculated from the simulated velocity and temperature are useful for evaluating whether 10^3m^2/s are small enough or not. The coefficient of eddy diffusion defined in terms of the gradient of time-averages and the correlation between the deviations from the time-averages of velocity components and temperature are calculated at each grid point for the four depths. They are negative at about half of the grid points. Their magnitudes, whether positive or negative, are much larger than 10^2m^2/s for momentum and 10^3m^2/s for heat, which suggests that the diffusion by the mesoscale eddies explicitly dealt with in the present study is much stronger than the eddy diffusion formulated in conventional Laplacian form with coefficients of 10^2m^2/s and 10^3m^2/s. This is also the case of the coefficient of vertical diffusion.

Another paper (YOKAYAMA and TAKANO, 1993) will present results of tracking of particles continuously or instantaneously released from a point source into the mesoscale eddies, which is another way to understand the effect of mesoscale eddies.

References

Atomic Energy Management Center (1986): Report of a preoperational survey of a proposed area for ocean disposal of radioactive wastes ——low-frequency water motion ——. 270pp. (in Japanese)

FRIEDRICH, H. and S. LEVITUS (1972): An approximation to the equation of state for sea water, suitable for numerical ocean models. J. Phys. Oceanogr., **2**, 514–517.

HAIDVOGEL, D, A.ROBINSON and C. ROOTH (1983): Eddy-induced dispersion and mixing. *in* Eddies in Marine Science (edit. by A. Robinson), 481–489, Springer-Verlag, Berlin, Heidelberg.

HAN, Y.J. (1975): Numerical simulation of mesoscale ocean eddies. Ph. D. thesis, Dept. Mete-

orol., UCLA, 153pp.
IMAWAKI, S. and K.TAKANO (1982): Low-frequency eddy kinetic energy spectrum in the deep western North Pacific. Science, **216**, 1407-1408.
OSTLUND, H. and K. BRESCHER (1982): GEOSECS Tritium. Univ. of Miami, Tritium Lab., Data Rept. No.12.
TAKANO, K. (1974): A general circulation model for the world ocean. Tech. Rept. No.8, Num. Simul. Weather and Climate, Dept. Meteorol., UCLA, 46pp.
TAKANO, K. (1982): Grid-size dependency of the meridional heat transport in a numerical model of an ocean. Atmos.-Ocean, **20**, 258-267.
YOKOYAMA, K. and K. TAKANO (1986): Relationship between the grid size and the coefficient of subgrid-scale diffusion in a finite difference advection-diffusion equation. La mer, **24**, 128-129.
YOKOYAMA, K. and K. TAKANO (1993) : Particle tracking in a mesoscale eddy field in an ocean. La mer, **31**, 75-86.

中規模うずによる受動追跡子の分散

横山恵子・高野健三

要旨：中規模うずが受動追跡子の分散に及ぼす影響を調べるための数値実験を行う。追跡子は移流と拡散によって広がる。流速は，4層の，うず分解大循環モデルから与えられる。海は緯度方向には25.0°Nから50.5°Nまでひろがる。経度方向のひろがりは24.8°である。南北方向に走る海嶺（海底からの高さは1900m）を除いて海の深さは一定（4000m）であり，北西太平洋の一部に似た形になっている。格子間隔は，緯度について0.375°，経度について0.43°である。三次元の移流・拡散方程式を時間積分して，追跡子の分布を80m，400m，1600m，2600mの深さで計算する。初期条件として，(i) 海面全体をおおう均一分布（瞬間面源）と (ii) 海底の一点だけの分布（瞬間点源）を与える。うずを含む流速場と，時間平均をとってうずを除いた平均流速場を使い，結果をくらべる。(i)，(ii) とも分散はうずによっていちじるしく速くなる。海全体に均一にひろがる（完全分散）までの時間は約30年で，平均流速を使うと約50年になる。完全分散に要する時間は海の体積にほぼ比例するだろうから，30年という長さは，世界中の海については約2300年，太平洋については約1250年に相当し，妥当な値になる。